AIAA 97-0768

Experimental and Computational Studies of the Flow Over a Sting Mounted Planetary Probe Configuration

M. Holden
Calspan-UB Research Center
Buffalo, NY

J. Harvey
Imperial College
London, UK

I. Boyd and J. George
Cornell University
Ithaca, NY

T. Horvath
NASA Langley Research Center
Hampton, VA

35th Aerospace Sciences Meeting & Exhibit
January 6-10, 1997 / Reno, NV

EXPERIMENTAL AND COMPUTATIONAL STUDIES OF THE FLOW OVER A STING MOUNTED PLANETARY PROBE CONFIGURATION*

Michael S. Holden†
Calspan-University at Buffalo Research Center
Buffalo, New York

John K. Harvey‡
Imperial College
Department of Aeronautics
London, UK

Iain D. Boyd§
Jyothish George¶
Cornell University
Ithaca, New York

Thomas J. Horvath#
NASA Langley Research Center
Hampton, VA

ABSTRACT

This paper summarizes the results of a series of experimental studies in the LENS shock tunnel and computations with DSMC and Navier Stokes codes which have been made to examine the aerothermal and flowfield characteristics of the flow over a sting-supported planetary probe configuration in hypervelocity air and nitrogen flows. The experimental program was conducted in the LENS hypervelocity shock tunnel at total enthalpies of 5 and 10 MJ/kg for a range of reservoir pressure conditions from 70 to 500 bars. Heat transfer and pressure measurements were made on the front and rear face of the probe and along the supporting sting. High-speed and single shot schlieren photography were also employed to examine the flow over the model and the time to establish the flow in the base recirculation region. Predictions of the flowfield characteristics and the distributions of heat transfer and pressure were made with DSMC codes for rarefied flow conditions and with the Navier-Stokes solvers for the higher pressure conditions where the flows were assumed to be laminar. Analysis of the time history records from the heat transfer and pressure instrumentation on the face of the probe and in the base region indicated that the base flow was fully established in under 4 milliseconds from flow initiation or between 35 and 50 flow lengths based on base height. The measurements made in three different tunnel entries with two models of identical geometries but with different instrumentation packages, one prepared by NASA Langley and the second prepared by CUBRC, demonstrated good agreement between heat transfer measurements made with two different types of thin film and coaxial gage instrumentation. The measurements of heat transfer and pressure to the front face of the probe were in good agreement with theoretical predictions from both the DSMC and Navier Stokes codes. For the measurements made in low density flows, computations with the DSMC code were found to compare well with the pressure and heat transfer measurements on the sting, although the computed heat transfer rates in the recirculation region did not exhibit the same characteristics as the measurements. For the 10 MJ/kg and 500 bar reservoir "match point" condition, the measurements and heat transfer along the sting from the first group of studies were in agreement with the Navier Stokes solutions for laminar conditions. A similar set of measurements made in later tests where the model was moved to a

* This program was supported under subcontract to the University of Southern California (USC) on Grant No. F49620-93-1-0373 and also USAMICOM under Contract No. SDIO84-93-C-0001. This paper is declared a work of the U.S. Government and is not subject to copyright protection in the United States.

† Research Fellow; Associate Fellow, AIAA
‡ Professor, Associate Fellow, AIAA
§ Associate Professor, Member, AIAA
¶ Graduate Research Assistant
# Aerospace Technologist

slightly different position in the test section indicated that the boundary layer in the reattachment compression region was close to transition or transitional where small changes in the test environment can result in larger than laminar heating rates. The maximum heating coefficients on the sting observed in the present studies was a small fraction of similar measurements obtained at nominally the same conditions in the HEG shock tunnel, where it is possible for transition to occur in the base flow, and in the low enthalpy studies conducted in the NASA Langley high Reynolds number Mach 10 tunnel where the base flow was shown to be turbulent. While the hybrid Navier-Stokes/DMSC calculations by Gochberg et al. (Reference 1) suggested that employing the Navier-Stokes calculations for the entire flowfield could be seriously in error in the base region for the 10 MJ/kg, 500 bar test case, similar calculations performed by Cornell, presented here, do not.

1. INTRODUCTION

Three years ago, as a result of discussions initiated in AGARD Working Group 18, an experimental program was conceived and designed to obtain measurements in a number of the major international high-enthalpy test facilities to examine the flow over a standardized test article at matched test points to compare and validate the performance of these facilities. The configuration selected as a standardized test article was a sting-mounted, blunted 70-degree cone with a flat base, which is shown in Figures 1 and 2. Measurements were to be obtained not only on the forebody but also on the base of the cone and along the sting. Thus, the rapid expansion region around the body perimeter, the wake and its associated shear layer reattachment process were all incorporated into the study. Each is recognized as being a severe challenge to current numerical prediction methods especially under conditions where real gas effects and possibly transition are present. Possibly it is for this reason this test case appears to have caught the imagination of many workers in the field. In a separate, but allied initiative, again associated with AGARD Working Group 18, experimental data was sought in low-density facilities to validate the calculations being made by various groups employing their DSMC codes. These two requirements were rolled into a test program which was conducted over a range of pressure conditions to obtain both low density and continuum flows at total enthalpies of 5 MJ/kg and 10 MJ/kg. Originally, three high-enthalpy facilities, the HEG, the LENS and the NASA Ames shock tunnel were involved in this program. However, subsequently, the test program in the Ames facility was replaced by studies in the low-enthalpy Mach 10 facility at NASA Langley, and measurements at the F4 facility in France. Thus, the sting-mounted planetary probe configuration has become a de facto standard for both the comparison and calibration of high-enthalpy facilities, and the evaluation of DSMC and Navier-Stokes codes designed to compute high-enthalpy flows with real gas effects.

In this paper, we present the measurements from three sets of studies conducted in the LENS facility with two models of the planetary probe configuration; the first instrumented by CUBRC and the second with instrumentation provided by NASA Langley. The planetary probe instrumented by Langley has now been tested in HEG, LENS, F4 and the Langley Mach 10 tunnel. In concert with the experimental program, detailed predictions were made by a number of researchers employing the DSMC and Navier-Stokes codes. In this paper, we present comparisons between these computations and the measurements made in the LENS facility. We first discuss the objectives and design of the experimental program. The LENS facility in which our experimental studies were conducted is described and its performance and calibration are briefly discussed. Details of the two planetary probe models used in the LENS studies are presented together with the instrumentation employed to measure the pressure, heat transfer, and flowfield characteristics. We then present and discuss the measurements made in the LENS facility. The time history measurements in the baseflow region are examined to provide information on the time establishment of the baseflow. These measurements are compared with time accurate solutions to the DSMC codes for low density flows. We then present and correlate the measurements from the three entries in the LENS facility and compare measurements for nitrogen and airflows to provide an indication of real-gas effects. We then present a series of comparisons between the experimental measurements and computations in the low density and continuum regimes with the DSMC and Navier-Stokes prediction methods. We also discuss the results of predictions employing hybrid Navier-Stokes/DSMC codes. Finally, we summarize the results from both the experimental and theoretical studies.

2. EXPERIMENTAL PROGRAM

2.1 Program Objectives and Design

The studies conducted with the planetary probe model are an important part of our program to calibrate and validate the performance of the LENS facility in high enthalpy flows. There were two main objectives of these studies. The first was to obtain surface and flowfield measurements at two sets of high enthalpy flow conditions, 5 MJ/kg and 10 MJ/kg at stagnation pressure levels of 500 bars for the specific purpose of comparing heat transfer and pressure distributions over the forebody and in the base region of identical models tested in the HEG, LENS, and F4 high-enthalpy tunnels under nominally identical flow conditions, as well as those conducted in the Langley low-enthalpy Mach 10 tunnel. The second objective was to obtain measurements in high temperature flows in both low density and continuum flow regimes, where vibrational relaxation and dissociation might influence the size and structure of separated base flow, for comparison with "state-of-the-art" DSMC and Navier-Stokes code solutions. The pressure levels selected for the facility comparison studies were set by the operational pressure limits of the AMES shock tunnel, while the 10 MJ/kg total enthalpy conditions was selected as a match point for all facilities and which corresponds to tailored - interface conditions in the LENS facility with a heated hydrogen driver.

2.2 Experimental Facilities

The LENS shock tunnel (Reference 2) is a chambered shock tunnel having a 24-foot-long driver tube with an internal diameter of 12 inches and a driven tube 8 inches in diameter, which is 60 feet long. The basic layout of the LENS facility is shown in Figure 3. The driver section of the tunnel is heated to 750°F and, because of hydrogen operation, is fitted with a stainless steel liner to prevent hydrogen embrittlement. The driver section of the tunnel can be operated at pressures up to 30,000 psi, and, because of its large volume, a high-pressure, high-flow-rate compressor was installed to provide a pumping capacity that will fill the driver in approximately one hour. The driver and heater section of the tunnel are mounted on carriages that recoil with the tunnel as it is fired. A double-diaphragm rig is used to initiate the flow. Here, two diaphragms are separated by an intermediate chamber, which is held at approximately half the driver pressure; the pressure in the intermediate chamber is rapidly increased to fire the tunnel. Diaphragms 18 inches in diameter and up to 1.25 inches thick are employed to obtain controlled bursts with the minimum amount of fragmentation. Because flowfield chemistry and cleanliness are of prime importance in this facility, driver and driven tube components that come into contact with the test gas are constructed from stainless steel. A centerbody apparatus, which employs a fast-acting plug valve to close the nozzle throat, is used to terminate the flow once the uncontaminated volume of shock-heated air has been exhausted from the reservoir region of the shock tube. The reservoir and centerbody region of the shock tunnel are lined with copper in order to prevent burning. Copper, molybdenum, or tungsten can be used for the throat section of the tunnel to prevent melting and burning. Because the high heating rates generated in the nozzle are concentrated in a relatively small region close to the throat, the major portion of the contoured nozzle can be constructed from fiberglass. To handle the large loads generated by the recoil of the tunnel, a metal corset, which surrounds the fiberglass nozzle, is used to couple the driven tube with the test section. The test section has an internal diameter of 96 inches and has been constructed so that it can be coupled to nozzles with exit planes up to 72 inches in diameter.

2.3 Planetary Probe Model and Instrumentation

The two models of the planetary probe configuration employed in this test program were identical in size and geometry. A schematic diagram of the planetary probe configuration is shown in Figure 2. A schematic diagram of the installation of the planetary probe model for the first and second entries into the LENS facility is shown in Figure 4. A photograph showing the positions of the instrumentation on the sting of the model is shown in Figure 5. The model used in the first three entries into the LENS facility was constructed by NASA Langley and the instrumentation was constructed, calibrated and installed by CUBRC. The second model used in the fourth entry was constructed and instrumented by NASA Langley (see Horvath-Reference 3) and employed coaxial thermocouple instrumentation on the front face and thin-film platinum gages deposited on a Macor substrate on the aft face and sting. The CUBRC instrumented model was equipped with thin-film heat transfer gages together with Medtherm coaxial thermocouples on the front face of the model and platinum thin-film instrumentation on the aft face and along the sting support system. To enable us to accurately examine the time establishment of the base flow region, a significant fraction of the

instrumentation was concentrated along the sting so that the length and structure of the reattachment compression region could be accurately resolved. Because of the cleanliness of the flow in the LENS facility under the high enthalpy conditions employed in these studies, we were able to employ magnesium fluoride-coated thin film heat transfer gages on the front face of the model without experiencing significant gage erosion. The addition of the Medtherm coaxial gages enabled us to examine and evaluate potential catalytic wall effects. The very low heating rates which we obtained on the sting in the low density studies (less than 0.1 BTU/ft^2/sec), required the use of special low-noise circuitry coupled with high-quality amplifiers.

The thin film instrumentation employed in these studies is capable of measuring heat transfer rates from 0.1 to 1000 Btu/ft^2/sec with a precision of between three and five percent. Each gage was calibrated to determine its temperature coefficient and resistance prior to the studies. The properties of the Pyrex were determined from pulse heating studies for a range of temperatures, and this variation is shown in Figure 6. The Stanton number, C_h, based on the freestream conditions, was calculated from the following expression,

$$C_h = \frac{\dot{q}}{\rho_\infty U_\infty (H_o - H_w)} \qquad (1)$$

where H_O and H_W are the total enthalpy of the free stream and the air at the wall.

The pressure transducers used in this program were piezoelectric types of a design developed by Calspan and manufactured by PCB Piezotronics, Inc. (Models 103A and 103M14). These sensors have high sensitivity, and linearity generally better than 2 percent, over an operating range of about four orders of magnitude. If the linearity was not within 2%, a log-log curve fit was made to the calibration data, and this resulted in all data being within 2% of the curve. The Model 103A transducers have a maximum pressure capability of 3 psi. The Model 103M14 transducers have a maximum capability of 100 psi. The transducers are internally compensated for acceleration to a nominal level of 0.001 psi/g.

The values of the pressure coefficients, C_p, were calculated from

$$C_p = p / \left(1/2 \rho_\infty U_\infty^2\right) \qquad (2)$$

The uncertainties in the pressure measurements associated with the calibration and recording apparatus were ±3%.

2.4 Flow Visualization

In addition to time-resolved surface measurements, high-speed movies were made with a Fastex camera running at approximately 8,000 frames/sec to examine time establishment and flow steadiness.

2.5 Data Recording and Reduction

All data were recorded on the 128-channel Calspan Digital Data Acquisition System (DDAS II). The DDAS II system consists of 128 Marel Co. Model 117-22 amplifiers, an Analogic ANDS 5400 data acquisition and distribution system, and a Sun SparcStation 2 computer. The Analogic system functions as a transient-event recorder in that it acquires, digitizes, and stores the data in real time. Immediately after each test run, the data was transferred to the Sun computer for processing. The Marel amplifiers provide gains up to 1000 for low-level signals, can be AC or DC coupled to the transducers, and have selectable low-pass filters with cutoff frequencies of 300, 1000, or 3000 Hz. The Analogic system contains a sample-and-hold amplifier, a 12-bit analog-to-digital converter, and a 4096-sample memory for each channel.

3. RESULTS AND DISCUSSION

3.1 Introduction

The test program for the planetary probe configuration was conducted with four entries into the LENS facility. Early in the first entry, it was found that the sting instrumentation, which was positioned based on pretest Navier-Stokes predictions, did not extend far enough downstream to encompass the entire length of the reattachment process. The model was immediately reinstrumented and measurements were obtained for a range of pressure levels at total enthalpies of 5 MJ/kg and 10 MJ/kg. The third entry was made with the same model, but with additional instrumentation added to the front face and along the sting to more accurately define the distribution of properties on the front face and base region of the model. For this entry, the model support system was further modified to minimize the potential upstream influence of the support system. In this and the subsequent study, the model was supported in a slightly different position in the test section. In the fourth and final entry, we

employed the planetary probe model, constructed and instrumented by NASA Langley. This was the identical model used in earlier studies in the HEG, (Reference 4) and NASA Langley (Reference 3) Mach 10 wind tunnel, and subsequently, in the F4 facility in France. The objective of this latter study was to repeat the measurements made at the conditions employed in the earlier studies with a completely different set of instrumentation to ensure that there were no issues associated with the measurement technique.

3.2 Test Conditions

The experimental studies in the LENS facility were conducted at six test conditions. Measurements were made for a total enthalpy level of 5 MJ/kg for reservoir pressures of 73, 290, and 500 bars with both air and nitrogen as the test gas.

In the first of the test cases (test condition B), the reservoir conditions were selected to achieve low density flows so that direct comparisons could be made between measurements of heat transfer on the forebody and in the base region of the planetary probe with computations using the DSMC code. The freestream conditions for test case B are listed in Table I. The conditions for test cases C and D were selected to achieve conditions where it was believed that computations employing either the Navier-Stokes codes or the DSMC computations could provide valid predictions for the flow. Here, air and nitrogen were used as the test gas for test case C and D, respectively, to examine potential real-gas effects and the freestream conditions calculated for these two test cases are listed in Tables II and III. The density levels for test cases A, E and F were such that fully continuum flow was developed in the forebody and base regions, and only Navier-Stokes or Navier-Stokes/DSMC hybrid methods could be practically employed to predict these flows. In fact, as discussed later, the Reynolds numbers developed under these conditions were large enough that transition from laminar to turbulent flow may have occurred in the reattachment compression region of these flows. Test conditions for test cases A, E, and F are listed in Tables IV, V and VI. The exact test conditions for each run, together with tabulations of the measurements, are presented in the CUBDAT database described in Reference 5 which is available from the first author on a CD-ROM.

3.3 Presentation and Discussion of the Experimental Measurements

During this test series, measurements were made over a range of Reynolds number for total enthalpies of 5 MJ/kg and 10 MJ/kg. At the key test conditions, we ran repeat runs for each entry into the facility employing the Calspan-instrumented model during the first three entries and the NASA-instrumented model during the fourth entry. The measurements obtained at condition A on the forebody and base region are shown for Run 9 in Figures 7a and 7b and for Run 32 in Figure 8. Comparisons of these two sets of data are shown in Figure 9. Pressure and heat transfer measurements on the forebody and sting of the CUBRC-instrumented planetary probe model for the Case B test conditions are shown in Figures 10 and 11. There were no measurements made at this condition with the NASA-instrumented model. The two sets of measurements obtained for the test condition C with the CUBRC-instrumented model are shown in Figures 12a, b and 13a, b. The pressure and heat transfer measurements obtained at a similar reservoir condition, but with nitrogen as the test gas (condition D) are shown in Figures 14 and 15. Comparisons between the measurements with air and nitrogen as the test gas are shown in Figures 16 and 17 and indicate that at these low enthalpy conditions, real-gas effects (vibrational non-equilibrium, oxygen dissociation and the NO "shuffle" reactions) do not play an important role. The measurements of pressure and heat transfer obtained at the "match point" E condition with the CUBRC-instrumented model, runs 22 and 29 are presented in Figures 18 a, b and 19 a, b, and those with the NASA Langley-instrumented model are shown in Figures 20 and 21. A comparison between the two sets of measurements are presented in Figures 22 a, b. Next in Figures 23 a, b, we present the measurements obtained on the CUBRC- and NASA-Langley instrumented models in runs 26 and 34 respectively at the "match point" with nitrogen as the test gas. Comparisons between the measurements obtained on the models with two different instrumentation sets are shown in Figures 24 a, b and 25 a, b . The comparisons between the air and nitrogen data at condition E and F indicate that the baseflows are not strongly influenced by real-gas effects. A comparison between the measurements made in the LENS facility and those in the HEG shock tunnel, (Reference 4) in Figure 26, suggest that transition in the baseflow region may significantly influence the size of the recirculation region and the peak heating that occurs along the sting. Questions associated with transition could be explored if further studies

were conducted at lower Reynolds numbers in the HEG facility.

3.4 Flow Visualization From High Speed Schlieren Photography

A sequence of photographs obtained with high-speed photography at 8,000 frames/sec and showed that bow shock was established over the model in less than 1 millisecond and remained perfectly steady for a run time of approximately 6 milliseconds. Because of the low density of the flow in the base region, we were unable to resolve the reattachment compression process with high-speed film.

3.5 Test Time and Flow Establishment

The flow establishment in regions of attached and separated flows have always been a subject of interest to the experimentalist performing studies in facilities with short flow durations. The clean and rapid start of a well-tailored shock tunnel provides an excellent facility to obtain information on the mechanism of flow establishment for separated flows which take longer than the approximately 1 millisecond that it takes to establish the flow through the tunnel nozzle. Past studies have correlated measurements of flow establishment in terms of number of flow lengths based on a characteristic length. Typical attached laminar and turbulent boundary layers take between 1.5 and 3 flow lengths (based on the characteristic length and freestream velocity) to establish. The establishment time for regions of laminar separated flows induced by compression corners and incident shocks can be as large as 10 to 20 flow lengths. However, some of the longest flow establishment times which have been observed are those associated with laminar base flow regions and here flow length based on body diameter of between 25 and 50 have been recorded.

In the present study the records from the forebody and base region instrumentation provided us with the opportunity to examine the time and mechanism for flow establishment of the baseflow region. A typical set of time history records from pressure and heat transfer instrumentation on the forebody and in the base region for the 5 MJ/kg and 500 bar reservoir conditions are shown in Figure 27. The pressure and heat transfer records on the face of the planetary probe indicate that the flow is established within the time to establish the steady flow in the tunnel, and there is a steady test time of up to 8 milliseconds. The end of the test time coincides with the arrival of the expansion fan causing a distinctive decrease in the pressure and heat transfer. The pressure records on the aft face of the cylinder indicate a slow rise to a plateau region taking approximately 3 milliseconds. The heat transfer to the aft face of the probe rises rapidly during the flow starting process and decreases to a slightly lower level as the baseflow region becomes established in approximately four milliseconds after flow initiation through the tunnel. The pressure records along the sting indicate that the flow well downstream of the reattachment compression region establishes quickly, but there is a slight increase in the pressure on the sting as the baseflow region increases slightly in size to reach a stable condition. This behavior is more graphically illustrated by observing the pressures ahead and downstream of the reattachment point. Upstream of reattachment, the pressure along the sting in the separated region rises as the shear layer moves slightly downstream during flow establishment. For pressure gages located initially downstream of the reattachment point, we observe an initial peak followed by a rapid decay in pressure to a steady level which again occurs approximately four milliseconds after flow initiation or close to 13 milliseconds after the initiation of data recording. The heat transfer measurements along the sting show similar trends to those obtained with the pressure instrumentation. Well downstream of reattachment, there is an increase in heat transfer to reach a steady level whereas in the baseflow region, the heat transfer decreases to a steady level as the flow in the base region becomes fully established. The formation of a steady flow in the base region can also be examined by plotting the distribution of pressure along the sting as a function of time as shown in Figure 28. The pressure distributions for time intervals from 11.5 milliseconds to 17 milliseconds after the initiation of data recording illustrates that the separated region grows in size to reach a stable condition within four milliseconds from data rise. The growth of the separated region reduces the maximum pressure and heat transfer which is recorded in the reattachment region.

A similar set of measurements along the sting obtained for the 10 MJ/kg, 500 bar reservoir condition are shown in Figures 29 and 30. Again, it can be observed that the separated region grows during flow establishment with a significant reduction in the heating levels in the reattachment compression region. Calculations to examine the time-establishment of a baseflow region for the 5 MJ/kg flow condition were made by Gallis and Harvey using the Imperial College Maximum Entropy DSMC code (Reference 6). The development of the distribution of heating along the sting as a function of time is presented in Figure 31. It can be seen that steady values of the heat transfer

along the sting are not reached until over 2 milliseconds after flow initiation. The predictions of the density contours in the baseflow region shown in Figures 32 a, b and 33 a, b also illustrate that it takes a significant time to establish the flow. From these figures, we can identify from the 0.3 contour changes in the size of a recirculation immediately behind the body which has taken 3 milliseconds to reach a steady state. The reattachment shock can be identified by the cluster of 0.4 to 0.6 contours emanating from the sting. It is diffuse because of the low densities in the wake and it plays a dominant role in the formation of the sting boundary and hence on the heat transfer at and downstream of the reattachment point. The wake is a low density region and the flow entering it from the forebody will not be in equilibrium due to the rapid expansion around the rim. The flow establishment time is thus determined principally by the (a) convection of the flow in the recirculation region and (b) by the relatively slow real gas relaxation processes. Thus, both the experimental and theoretical studies indicate that it takes 50 flow lengths to establish a steady separated flow in the baseflow region of the planetary probe.

4. COMPARISONS BETWEEN MEASUREMENTS AND COMPUTATIONS WITH THE DSMC AND NAVIER-STOKES CODES

4.1 Introduction

During the course of this work, a number of calculations have been performed by a number of researchers in the U.S. and Europe to compare with the measurements made on the planetary probe in the LENS facility. For the measurements in low-density flows where the DSMC computational technique can yield accurate results, calculations were made by Moss, (Reference 7) Harvey and Gallis (Reference 8) and Dietrich and Boyd (Reference 9). For the 5 MJ/kg and 10 MJ/kg test cases at the 500 bar reservoir condition, calculations have been made at Cornell with a Navier-Stokes code and a hybrid Navier-Stokes/DSMC method, by Hash et al., (Reference 10) Muylaert (Reference 11) and Chadwick (Reference 8) using different Navier-Stokes solvers. The initial series of studies were designed to provide information for fully laminar conditions over the sting-mounted planetary probe configuration for direct comparison with solutions from DSMC and Navier-Stokes codes and were selected so that there could be some overlapping over the range of applicability of these two prediction techniques. Measurements were then made at higher Reynolds numbers were transition is believed to occur in or downstream of the baseflow region. It is in these latter studies that the test case E, which is the 10 MJ/kg and 500 bar reservoir condition, falls.

4.2 Comparison Between Measurements with DSMC Predictions

For the lowest Reynolds number case, the flow in the forebody and base region is non-continuum and the DSMC solution technique can be readily employed to predict the flows over the planetary probe. The first comparisons made with the pressure and heat transfer measurements for the test case B condition were obtained by Moss (Reference 7) Gallis and Harvey (Reference 8) and Dietrich and Boyd are shown compared with the data in Figures 34 a, b and 35 a, b. It can be seen from these figures, that both sets of computation are in relatively good agreement and predict the features of pressure and heat transfer distribution in the baseflow region. However, while the theories are in good agreement with the measurements on the forebody, they slightly overpredict the pressure and heat transfer in the recompression region over the sting. Increasing the Reynolds number to obtain conditions close to the continuum regime over the forebody and the base region enables a comparison to be made between solutions obtained by Harvey and Gallis (Reference 8) with the DSMC code and Hash et al. (Reference 10) with their Navier-Stokes based prediction method. These comparisons are shown in Figures 36 and 37 for the pressure and heat transfer measurements made at the LENS case C and D test conditions for the same nominal air conditions with air and nitrogen as the test gas, respectively. Again, the measurements with nitrogen and air as the test gas indicate that real-gas effects were insignificant in these flows. Here the prediction methods do not agree well in the baseflow region, but give comparable results downstream of reattachment. Neither computations predict the slower pressure and heat transfer rise measured in the recompression region of the baseflow.

4.3 Comparison Between Measurements with Navier-Stokes Predictions

An important set of comparisons were those between Navier-Stokes solutions and the measurements obtained for LENS cases E and F, which are at the 10 MJ/kg enthalpy and 500 bar reservoir conditions with air and nitrogen as the test gas, respectively. Test case E was developed as a match point between the various hypervelocity facilities in which the planetary probe has been tested. In particular,

measurements have been obtained in the HEG and LENS shock tunnels and the "hot shot" facility Tunnel F in France at the nominal 10 MJ/kg and 500 bar test case with air. Because of the high density levels at which these studies were conducted, the flow over the front face and in the majority of the wake can be considered as fully continuum, and solutions based on the Navier-Stokes equations provide the only practical prediction technique. However, in the expansion region above the separated baseflow, the densities may be low enough that the assumption in such computations are invalid, and in this region the DSMC code could be more applicable. Therefore, calculations employing the Navier-Stokes code to compute the forebody flow coupled with a DSMC method to compute the base region have been pursued. Navier-Stokes solutions to compute the flow over the planetary probe configuration for case E test conditions have been obtained by Muylaert et al. (Reference 11) Chadwick (Reference 8) and at Cornell. Computations using the hybrid Navier-Stokes/DSMC method have been obtained by Gochberg (Reference 1) and again at Cornell. Comparisons between the calculations of heat transfer and pressure obtained by Muylaert et al. (Reference 10) using the TINA code are compared with measurements of heat transfer rate for Run Nos. 22, 29, and 33 are shown in Figure 38. The computations are in excellent agreement with the experimental measurements on the front face of the probe, but fall slightly below the measurements downstream of the reattachment region on the sting. As discussed earlier, we believe that for Run Nos. 29 and 33, the heating levels downstream of the reattachment region may be influenced by the beginning of a transition process. A similar set of comparisons for the computations employing the GASP code (Reference 12) performed by Chadwick is shown in Figure 39. Here the computations fall slightly above the measurements during the recompression process along the sting. Finally, in Figures 40 and 41, we show the comparisons between the heat transfer and pressure measurements and computations performed at Cornell using a Navier-Stokes computation. Again, we see that while predictions for the forebody are in good agreement with the measurements, the flow in the recompression region is not well predicted and the measurements fall above the predictions downstream of the recompression region on the sting. Although discrepancies may occur between individual computations due to incorrect implementation, the differences may also illustrate a general potential weakness of the continuum codes in handling flows in which there are very rapid expansions such as that that occurs around the rim of this configuration. In this instance, a failure to compute the localized flow in the region of the rim will set inappropriate upstream conditions for the wake and reattachment flow computations where the discrepancies may be amplified.

4.4 Discussion of Predictions with Hybrid Prediction Scheme

Citing problems with the validity of employing the Navier-Stokes code in the wake regions of these flows, Gochberg et al. performed computations using a hybrid method where a Navier-Stokes solution for the forebody was joined with a DSMC calculation in the wake region. Two cases were calculated: (1) the LENS case E and (2) the HEG Run 132. Again, the computations were in good agreement with the experimental measurements from the HEG and LENS facility on the forebody as shown in Figure 42. However, in the baseflow, the hybrid solution predicted large levels of heating in the reattachment compression region, which more closely agreed with those obtained in the HEG facility. Measurements in the LENS facility were lower by a factor between 3 and 5 as shown in Figure 43. In a companion calculation, the flows were computed with a full Navier-Stokes solution employing the NEQ2D code. These predictions indicated that the separated region was significantly shorter than that found in experiment, although the peak heating levels in the reattachment region were comparable. The Navier-Stokes predictions in this paper were not in good agreement with those obtained earlier by Muylaert and Chadwick. The relatively poor agreement between the hybrid predictions and the experimental data prompted additional efforts employing a decoupled Navier-Stokes/DSMC approach at Cornell. Comparisons between the pressure and heat transfer measurements for the LENS case E condition with computations employing the hybrid technique and the Navier-Stokes/DSMC computation for the boundaries illustrated in Figure 44 are shown in Figures 45 and 46. Here it can be seen that unlike the earlier predictions by Gochberg et al. (Reference 1), the two prediction techniques do not significantly differ, although the predictions at the end of the reattachment region employing the hybrid code are in better agreement with experiment. Again, the pressure measurements has exhibited a slower return to the sting pressure than predicted by either the Navier-Stokes or hybrid codes. Clearly, further investigations are required to examine the discrepancies between the results of the two hybrid computational methods and to explore the factors

which influence the accuracy of the Navier-Stokes codes in regions of highly-expanded flow.

5. SUMMARY AND CONCLUSIONS

Experimental studies and computations with the DSMC and Navier-Stokes codes have been made to examine the aerothermal and flowfield characteristics of the flow over a sting mounted planetary probe configuration in hypervelocity air and nitrogen flows. In the experimental program, conducted in the LENS hypervelocity shock tunnel, surface and flowfield measurements were made at total enthalpies of 5 MJ/kg and 10 MJ/kg for a range of reservoir pressures from 70 to 500 bars. Heat transfer and pressure measurements were made with separate sets of instrumentation constructed and calibrated by CUBRC and NASA Langley, respectively. The heat transfer and pressure measurements made with these two different sets of instrumentation installed on the front and rear face of the probe and along the sting on the two models of identical geometry were in excellent agreement. High-speed and single shock Schlieren photography were also employed to examine the flow over the model and the time to establish the flow in the base region. Analysis of the time history measurements of the heat transfer and pressure indicated that the baseflow was fully established within 4 milliseconds of flow initiation or between 35 and 50 flow lengths based on freestream velocity and base height. Time accurate calculations with the DSMC code were in agreement with these flow establishment times. Computations employing the DSMC code were found to compare well with the pressure and heat transfer measurements over the model and sting under rarefied flow conditions. Navier-Stokes solutions assuming continuum, laminar flow for the 10 MJ/kg and 500 bar reservoir conditions, were in agreement with the measurements on the probe and along the sting. The maximum heating coefficients on the sting observed in the present studies was a small fraction of similar measurements obtained at nominally the same conditions in the HEG shock tunnel, where it is possible transition occurred in the baseflow, and in the low enthalpy studies conducted in the NASA Langley high Reynolds number Mach 10 tunnel where the baseflow was shown to be turbulent. Measurements of sting heating in the LENS facility indicate that the flow in the base recompression region is close to transitional at the match point conditions. Although the hybrid Navier-Stokes/DSMC calculations performed by Gochberg suggested that Navier-Stokes calculations could be seriously in error in the baseflow region, similar Navier-Stokes/DSMC calculations presented here by Dietrich and Boyd, did not.

6. REFERENCES

1. Gochberg, L.A., Allen, G.A., Gallis, M.A. and Deiwert, G.S., "Comparison of Computations and Experiments for Nonequilibrium Flow Expansions Around a Blunted Cone," AIAA Paper No. 96-0231

2. Holden, M.S., "Large-Energy National Shock Tunnel (LENS) Description and Capabilities" Brochure, February 1991.

3. Horvath, T., McGinley, C., and Hannemann K., "Blunt Body Near Wake Flowfield at Mach 6," AIAA Paper No. 96-1935, New Orleans, LA.

4. Kastell, D., Horvath, T.J., and Eitelberg, G., "Nonequilibrium Flow Expansion Experiment Around a Blunted Cone," 4th European High Velocity Database Workshop ESTEC, Noordwijk, The Netherlands (1994).

5. Holden, M.S., Moselle, J.R., Sweet, S.J. and Martin, S.C., "A Database of Aerothermal Measurements in Hypersonic Flow for CFD Validation," AIAA Paper No. 96-4587, Norfolk, VA.

6. Gallis, M.A. and Harvey, J.K., (1995a) "Comparison of the Maximum Entropy DSMC Code with Flowfield Measurements," AIAA Paper 95-0413, 33rd Aerospace Sciences Meeting and Exhibit in Reno, NV, January 9-12.

7. Moss, J. N., Dogra, V. K., and Price, J. M., "DSMC Calculations for a 70° Blunted Cone at a 3.2 km/s Test Condition," NASA TM to be published in 1995.

8. Holden, M.S., Chadwick, K.M., Gallis, M.A. and Harvey, J.K., "Comparison Between Shock Tunnel Measurements on a Planetary Probe Configuration and DSMC Predictions," paper presented at the 20th International Symposium on Shock Waves at California Institute of Technology, Pasadena, July 23-28, 1995.

9. Dietrich, S. and Boyd, I.D., "A Scalar Optimized Parallel Implementation of the

DSMC Technique," *Journal of Computational Physics*, Vol. 126, 1996, pp. 328-342.

10. Hash, D. B., Hassan, H. A., Dogra, V. K., and Price, J. M., "Navier-Stokes Calculations for a Spherically Blunted Cone (LENS Condition)," Presented at the 4th European High-Velocity Database Workshop, ESTEC, Noordwijk, November 24-25, 1994.

11. Muylaert, J. Walpot, L., Spel, M., Tumino, G. and Steijl, R., "Non-Equilibrium Computational Analysis of Blunt-Cone Experiments Performed in the LENS and HEG Facilities, AIAA Paper No. 96-2436, New Orleans, LA.

12. McGrory, W. D., Slack, D. C., Applebaum, M. P., and Walters, R. W., "GASP Version 2.2 Users Guide," Aerosoft, Inc., Blacksburg, VA, 1992.

Table I. Test Condition B

Shock Mach Number	Mi	=	6.243
Reservoir Pressure	PO	=	1075. psia
Total Enthalpy	HO	=	5.798E+07 (ft/sec)**2
Stagnation Temperature	TO	=	7832. degrees R
Freestream Mach No.	M	=	15.63
Freestream Reynolds No.	Re	=	1.7461E+04 1/ft
Freestream Velocity	U	=	10649. Ft/sec
Freestream Temperature	T	=	186.7 degrees R
Freestream Pressure	P	=	5.84E-04 psia
Freestream Density	RHO	=	2.534E-07 slugs/ft/ft/ft
Pitot Pressure	Pitot	=	1.7914E-01 psia
Wall Temperature	Twall	=	5.2660E+02 degrees R
Molecular Weight	MW	=	28.005
	N2 mole fraction = .9996		
	N mole fraction = .0004		

Table II. Test Condition C

Shock Mach Number	Mi	=	6.364
Reservoir Pressure	PO	=	4222. psia
Total Enthalpy	HO	=	5.6466E+07 (ft/sec)**2
Stagnation Temperature	TO	=	7.0597E+03 degrees R
Freestream Mach No.	M	=	10.23
Freestream Reynolds No.	Re	=	2.7093E+05 1/ft
Freestream Velocity	U	=	1.0128E+04 Ft/sec
Freestream Temperature	T	=	4.0731E+02 degrees R
Freestream Pressure	P	=	4.0054E-02 psia
Freestream Density	RHO	=	8.2404E-06 slugs/ft/ft/ft
Pitot Pressure	Pitot	=	5.3966E+00 psia
Wall Temperature	Twall	=	5.3320E+02 degrees R
Molecular Weight	MW	=	28.94
	N2 mole fraction = 7.411E-01		
	N mole fraction = 4.710E-40		
	O2 mole fraction = 1.698E-01		
	AR mole fraction = 9.319E-03		
	O mole fraction = 1.181E-03		
	NO mole fraction = 7.859E-02		

Table III. Test Condition D

Shock Mach Number	Mi	=	6.4090
Reservoir Pressure	PO	=	4.2080E+03 psia
Total Enthalpy	HO	=	6.0915E+07 (ft/sec)**2
Stagnation Temperature	TO	=	8.2014E+03 degrees R
Freestream Mach No.	M	=	10.31
Freestream Reynolds No.	Re	=	2.3540E+05 1/ft
Freestream Velocity	U	=	1.0784E+04 Ft/sec
Freestream Temperature	T	=	4.4061E+02 degrees R
Freestream Pressure	P	=	3.8963E-02 psia
Freestream Density	RHO	=	7.1714E-06 slugs/ft/ft/ft
Pitot Pressure	Pitot	=	5.3249E+00 psia
Wall Temperature	Twall	=	5.3590E+02 degrees R
Molecular Weight	MW	=	28.01
	N2 mole fraction = 9.998E-01		
	N mole fraction = 1.882E-04		

Table IV. Test Condition A

Shock Mach Number	Mi	=	6.470
Reservoir Pressure	PO	=	7.5880E+03 psia
Total Enthalpy	HO	=	5.8402E+07 (ft/sec)**2
Stagnation Temperature	TO	=	7.2959E+03 degrees R
Freestream Mach No.	M	=	10.25
Freestream Reynolds No.	Re	=	4.4945E+05 1/ft
Freestream Velocity	U	=	1.0327E+04 Ft/sec
Freestream Temperature	T	=	4.2170E+02 degrees R
Freestream Pressure	P	=	6.9402E-02 psia
Freestream Density	RHO	=	1.3795E-05 slugs/ft/ft/ft
Pitot Pressure	Pitot	=	9.3927E+00 psia
Wall Temperature	Twall	=	5.3410E+02 degrees R
Molecular Weight	MW	=	28.95
	N2 mole fraction = 7.433E-01		
	N mole fraction = 2.266E-39		
	O2 mole fraction = 1.721E-01		
	AR mole fraction = 9.321E-03		
	O mole fraction = 6.002E-04		
	NO mole fraction = 7.469E-02		

Table V. Test Condition E

Shock Mach Number	Mi	=	9.258
Reservoir Pressure	PO	=	7.1230E+03 psia
Total Enthalpy	HO	=	1.1831E+08 (ft/sec)**2
Stagnation Temperature	TO	=	1.1653E+04 degrees R
Freestream Mach No.	M	=	8.6545
Freestream Reynolds No.	Re	=	1.3841E+05 1/ft
Freestream Velocity	U	=	1.4525E+04 Ft/sec
Freestream Temperature	T	=	1.1728E+03 degrees R
Freestream Pressure	P	=	9.0307E-02 psia
Freestream Density	RHO	=	6.3331E-06 slugs/ft/ft/ft
Pitot Pressure	Pitot	=	8.5888E+00 psia
Wall Temperature	Twall	=	5.3570E+02 degrees R
Molecular Weight	MW	=	28.41
	N2 mole fraction = 7.357E-01		
	N mole fraction = 5.763E-11		
	O2 mole fraction = 1.564E-01		
	AR mole fraction = 9.146E-03		
	O mole fraction = 3.816E-02		
	NO mole fraction = 6.056E-02		
	NO+ mole fraction = 9.287E-09		
	E- mole fraction = 9.287E-09		

Table VI. Test Condition F

Shock Mach Number	Mi	=	8.8590
Reservoir Pressure	PO	=	7.3620E+03 psia
Total Enthalpy	HO	=	1.1193E+08 (ft/sec)**2
Stagnation Temperature	TO	=	1.3033E+04 degrees R
Freestream Mach No.	M	=	9.3017
Freestream Reynolds No.	Re	=	1.6294E+05 1/ft
Freestream Velocity	U	=	1.4505E+04 Ft/sec
Freestream Temperature	T	=	9.8599E+02 degrees R
Freestream Pressure	P	=	8.1132E-02 psia
Freestream Density	RHO	=	6.6629E-06 slugs/ft/ft/ft
Pitot Pressure	Pitot	=	8.9795E+00 psia
Wall Temperature	Twall	=	5.3380E+02 degrees R
Molecular Weight	MW	=	27.97
	N2 mole fraction = 9.968E-01		
	N mole fraction = 3.186E-03		

Figure 1 70° Cone Section of Planetary Probe

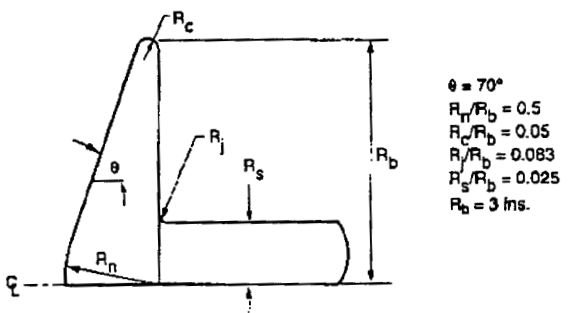

Figure 2 Blunt Body/Wake Closure Test Model

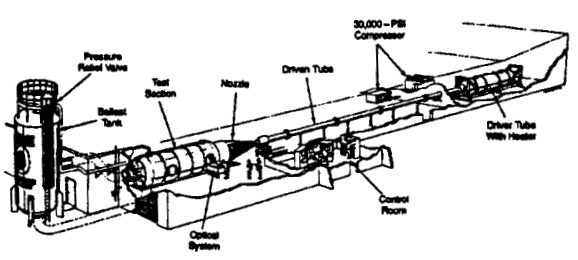

Figure 3 Large Energy National Shock Tunnel (LENS)

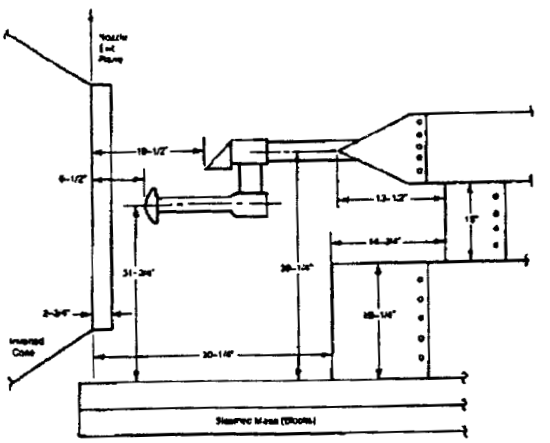

Figure 4 Diagram of Support Section and Sting Mount with Planetary Probe

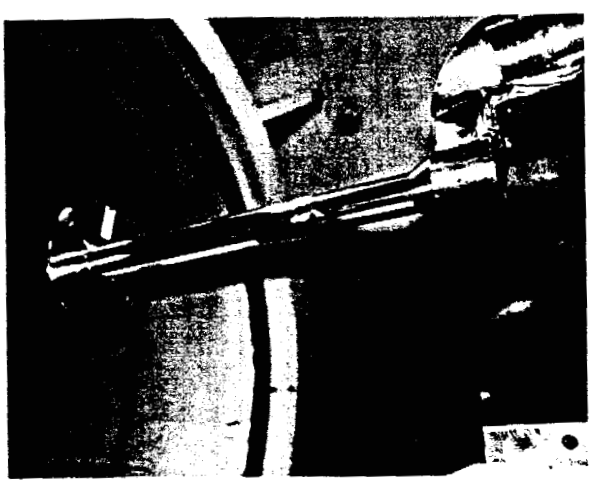

Figure 5 Planetary Probe Installed in LENS Tunnel

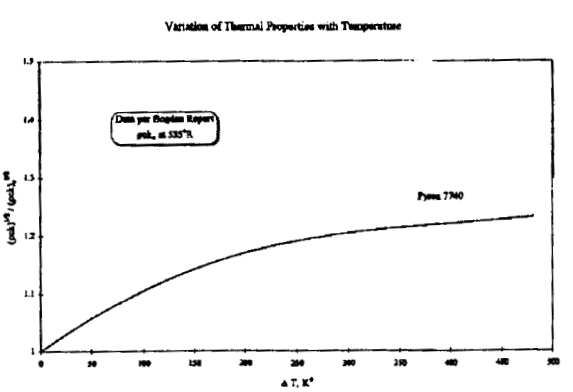

Figure 6 Variation of the Properties of the Pyrex Substrate with Temperature Employed in Heat Transfer Data Reduction Code

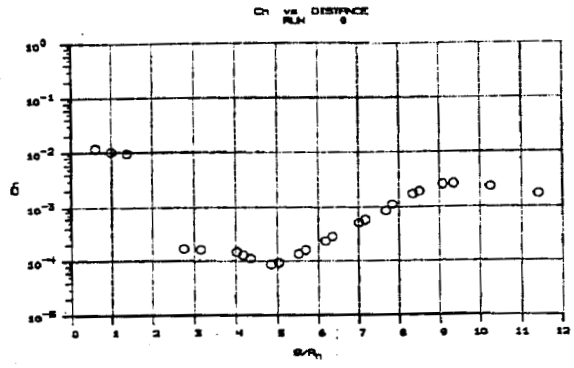

Figure 7a Distribution of Heat Transfer Coefficient over Planetary Probe Model and Sting for Case A Test Condition (Run 9)

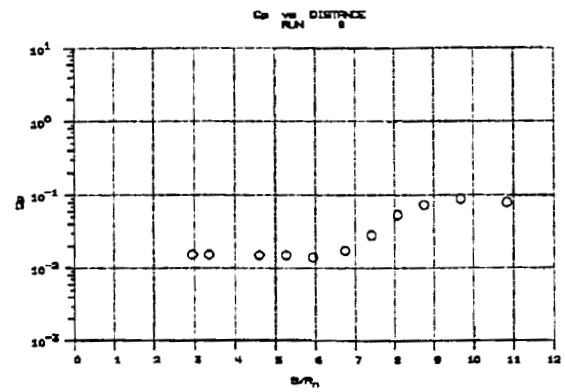

Figure 7b Distribution of Pressure Coefficient over Planetary Probe Model and Sting for Case A Test Condition (Run 9)

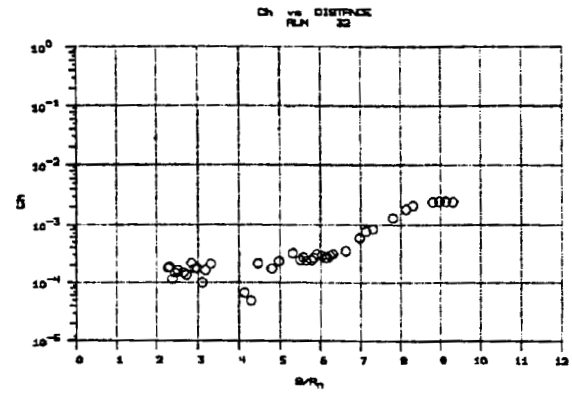

Figure 8 Distribution of Heat Transfer Coefficient over Planetary Probe Model and Sting for Case A Test Condition (Run 32)

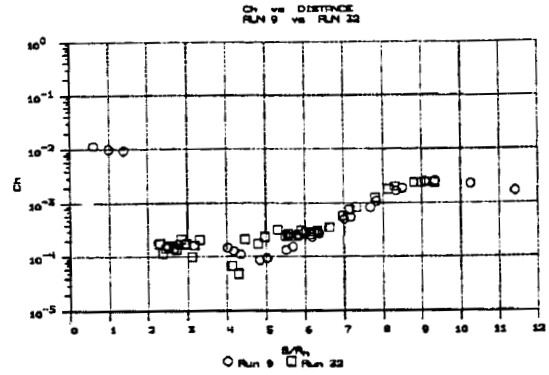

Figure 9 Comparison of Distributions of Heat Transfer Coefficient over Planetary Probe Model and Sting for Case A Test Condition for CUBRC and NASA Instrumented Models

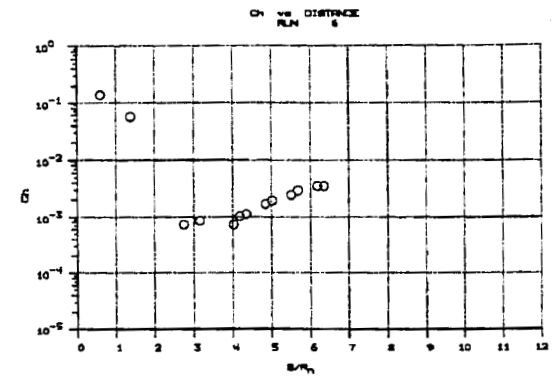

Figure 10 Distribution of Heat Transfer Coefficient Over Planetary Probe Model and Sting for Case B Test Condition (Run 6)

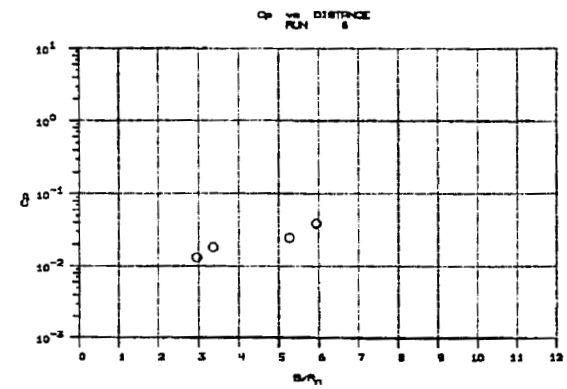

Figure 11 Distribution of Pressure Coefficient over Planetary Probe Model and Sting for Case B Test Condition (Run 6)

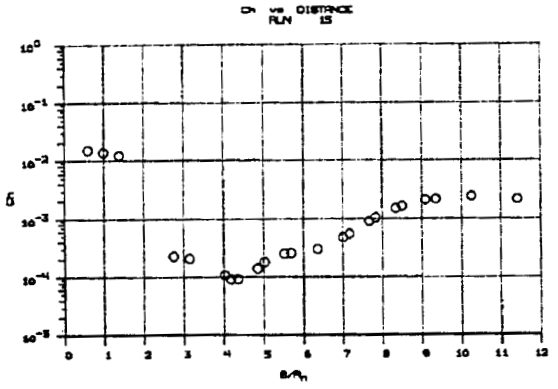

Figure 12a Distribution of Heat Transfer Coefficient over Planetary Probe Model and Sting for Case C Test Condition (Run 15)

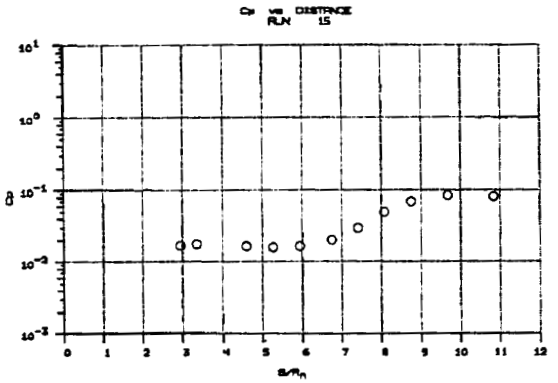

Figure 12b Distribution of Pressure Coefficient over Planetary Probe Model and Sting for Case C Test Condition (Run 15)

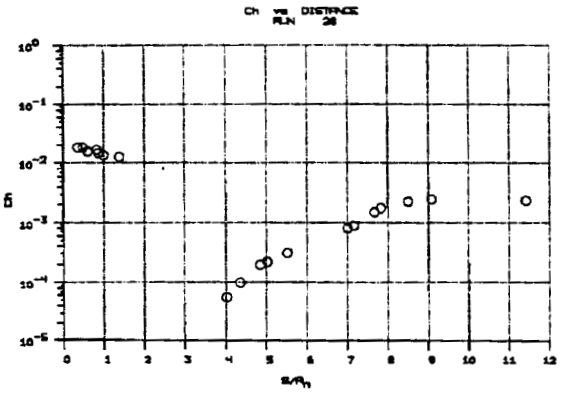

Figure 13a Distribution of Heat Transfer Coefficient over Planetary Probe Model and Sting for Case C Test Condition (Run 28)

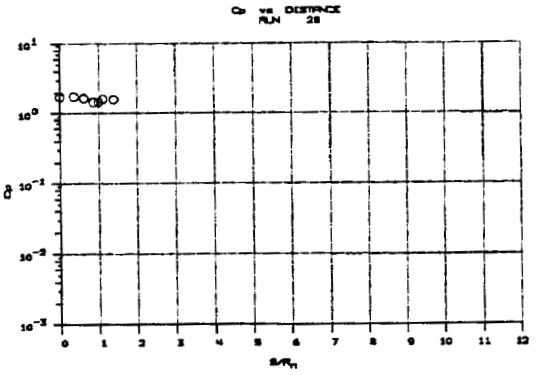

Figure 13b Distribution of Pressure Coefficient over Planetary Probe Model and Sting for Case C Test Condition (Run 28)

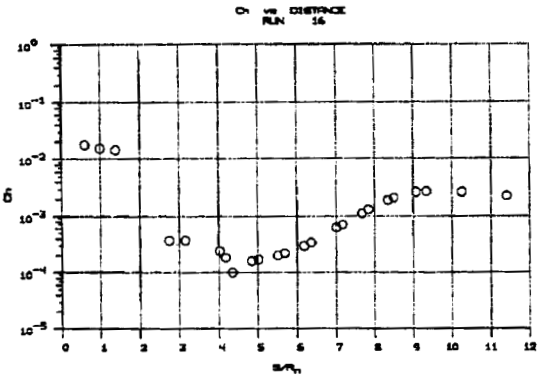

Figure 14 Distribution of Heat Transfer Coefficient over Planetary Probe Model and Sting for Case D Test Condition (Run 16)

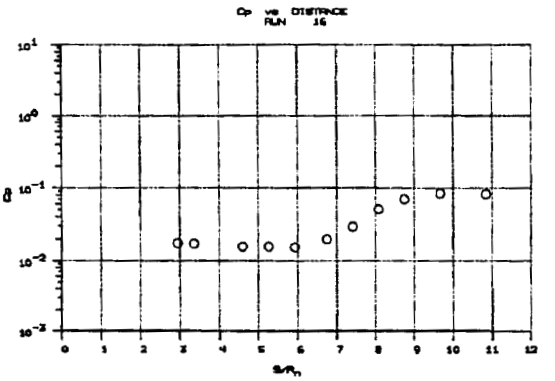

Figure 15 Distribution of Pressure Coefficient over Planetary Probe Model and Sting for Case D Test Condition (Run 16)

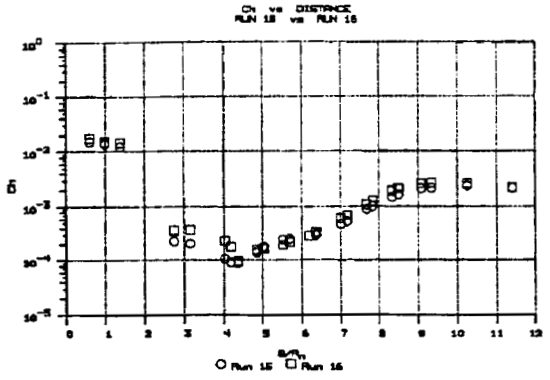

Figure 16 Comparison Between the Distribution of Heat Transfer Coefficient for Air and Nitrogen Flows for the 5Mj/kg, 500 Atmosphere Reservoir Condition

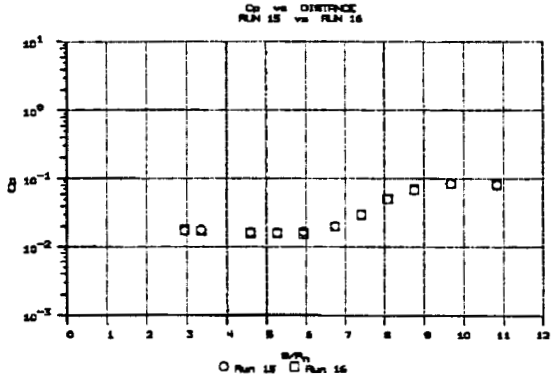

Figure 17 Comparison Between the Distribution of Pressure Coefficient for Air and Nitrogen Flows for the 5Mj/kg, 500 Atmosphere Reservoir Condition

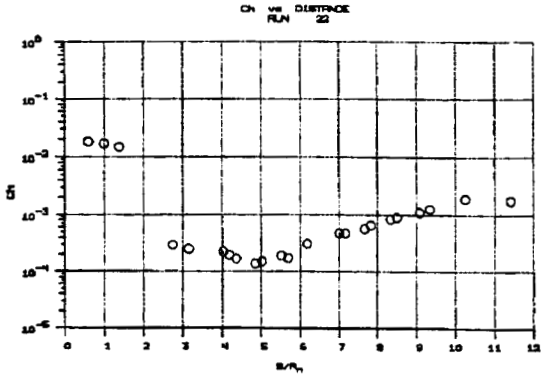

Figure 18a Distribution of Heat Transfer Coefficient over Planetary Probe Model and Sting for "Match Point" E Test Conditions (Run 22)

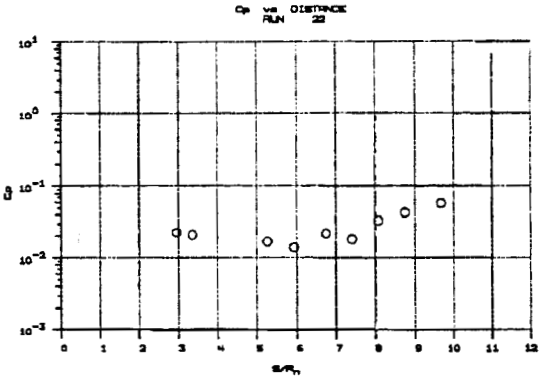

Figure 18b Distribution of Pressure Coefficient over Planetary Probe Model and Sting for "Match Point" E Test Conditions (Run 22)

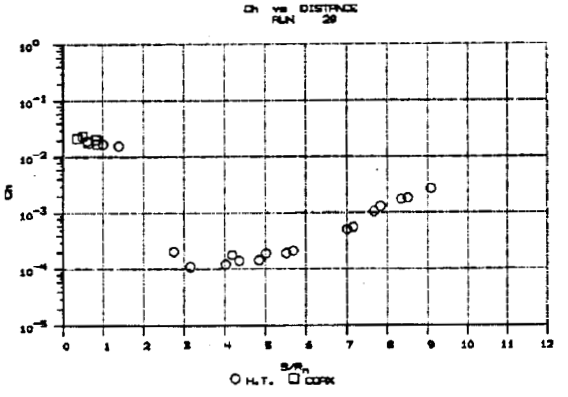

Figure 19a Distribution of Heat Transfer Coefficient over Planetary Probe Model and Sting for "Match Point" E Test Conditions (Run 29)

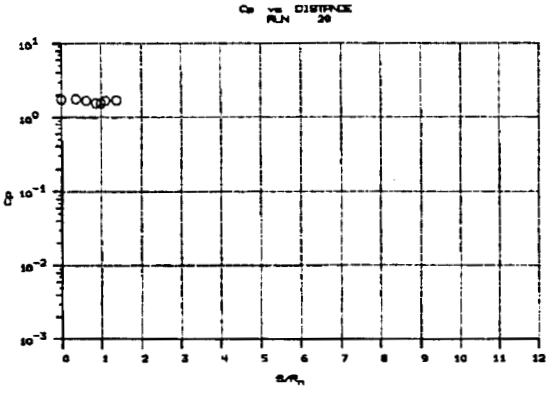

Figure 19b Distribution of Pressure Coefficient over Planetary Probe Model and Sting for "Match Point" E Test Conditions (Run 29)

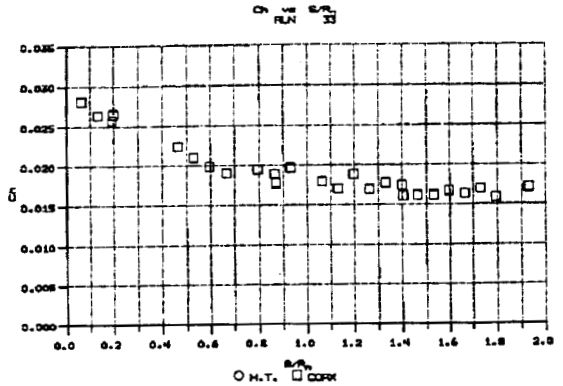

Figure 20 Distribution of Heat Transfer Coefficient on Front Face of Planetary Probe at "Match Point" E (Run 33)

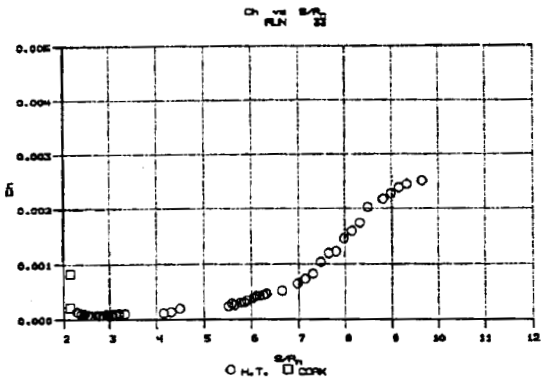

Figure 21 Distribution of Heat Transfer Coefficient on Rear Face and Sting of Planetary Probe at "Match Point" E (Run 33)

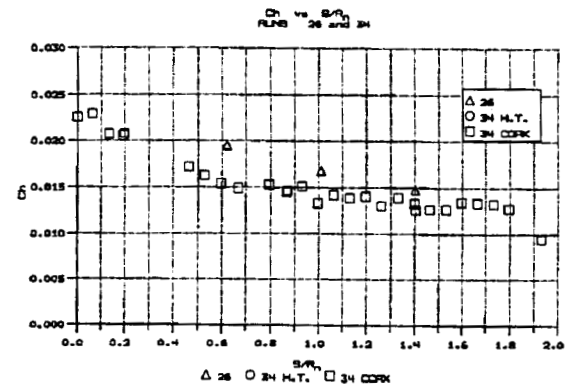

Figure 22a Comparisons Between the Distributions of Heat Transfer Coefficient on Front Face of Planetary Probe at "Match Point" E (Run Nos. 29 & 33) for CUBRC and NASA Instrumented Models

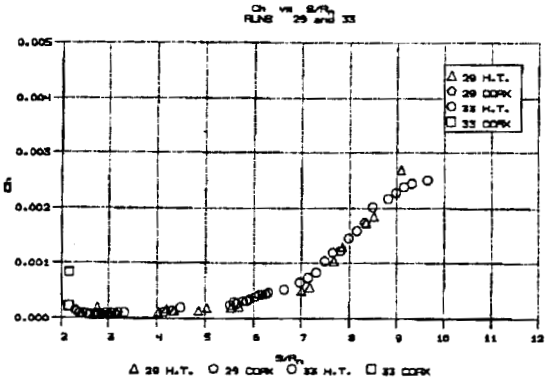

Figure 22b Comparison Between the Distributions of Heat Transfer Coefficient on Rear Face and Sting of Planetary Probe at "Match Point" E (Run Nos. 29 & 33) for CUBRC and NASA Instrumented Models

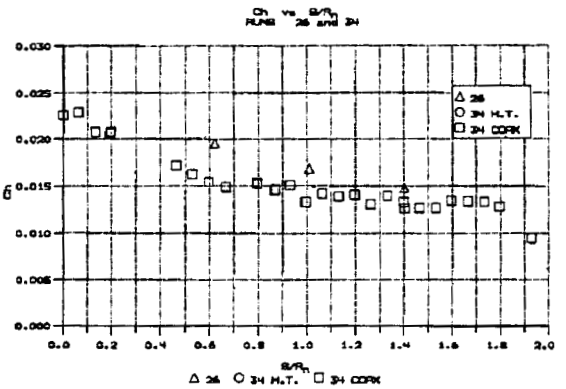

Figure 23a Distribution of Heat Transfer Coefficient on Front Face of Planetary Probe at "Match Point" E with Nitrogen Test Gas (Run Nos. 26 & 34) Test Condition F

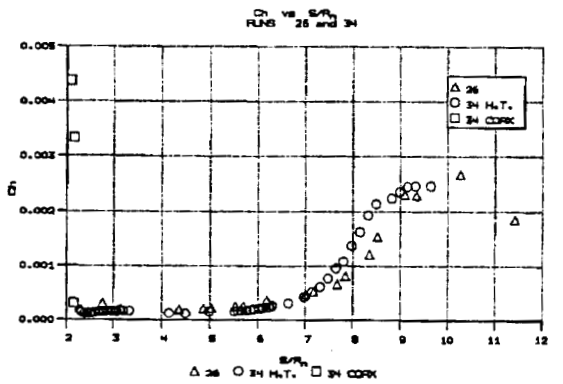

Figure 23b Distribution of Heat Transfer Coefficient on Rear Face and Sting of Planetary Probe at "Match Point" E with Nitrogen Test Gas (Run Nos. 29 & 33) Test Condition F

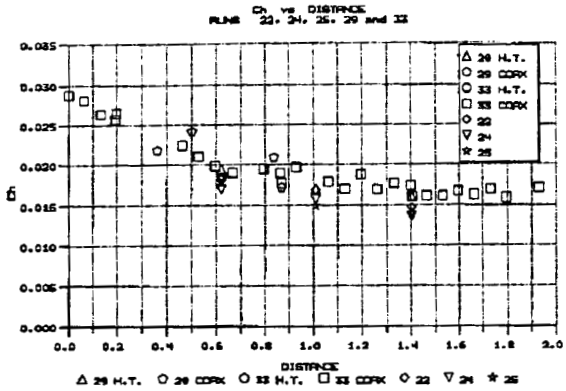

Figure 24a Comparisons Between all the Heat Transfer Distributions on the Front Face of the Planetary Probe at "Match Point" E (Run Nos. 22, 24, 25, 29 & 33) for CUBRC and NASA Instrumented Models

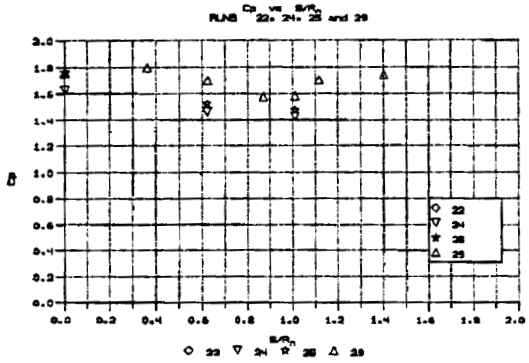

Figure 24b Comparisons Between all the Pressure Distributions on the Front Face of the Planetary Probe at "Match Point" E (Run Nos. 22, 24, 25, 29 & 33) for CUBRC and NASA Instrumented Models

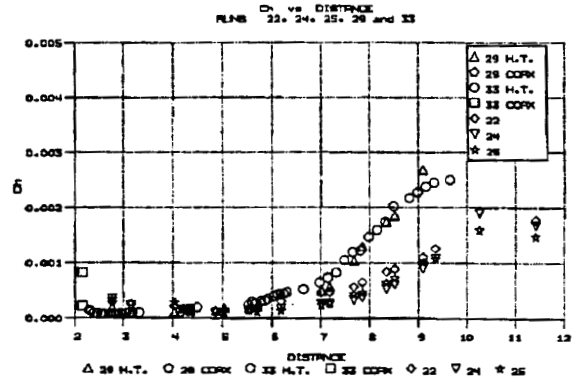

Figure 25a Comparisons Between all the Heat Transfer Distributions on the Rear Face and Sting of the Planetary Probe at "Match Point" E (Run Nos. 22, 24, 25, 29 & 33) for CUBRC and NASA Instrumented Models

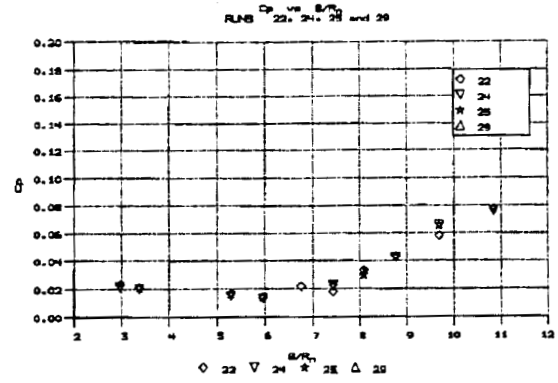

Figure 25b Comparisons Between all the Pressure Distributions on the Rear Face and Sting of the Planetary Probe at "Match Point" E (Run Nos. 22, 24, 25, 29 & 33) for CUBRC and NASA Instrumented Models

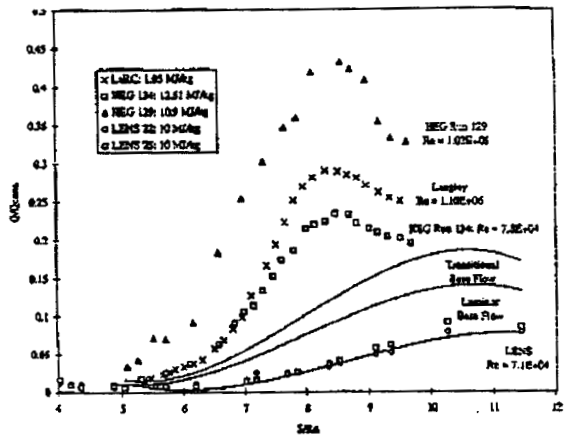

Figure 26 Comparison Between Measurements of Heat transfer Along the Sting Obtained in the LENS and HEG Shock Tunnels at the 10 Mj/kg Match Point

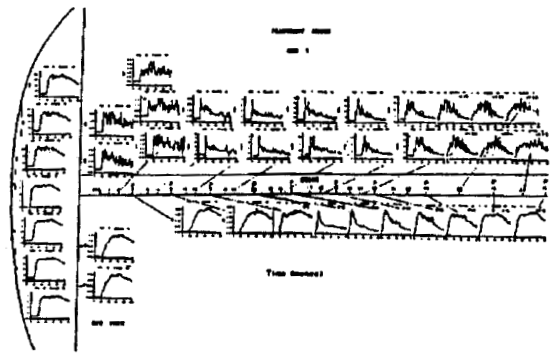

Figure 27 Time Establishment of Base Flow Over the Model and Sting - LENS Case A, 5 Mj/kg, 500 Atmospheres

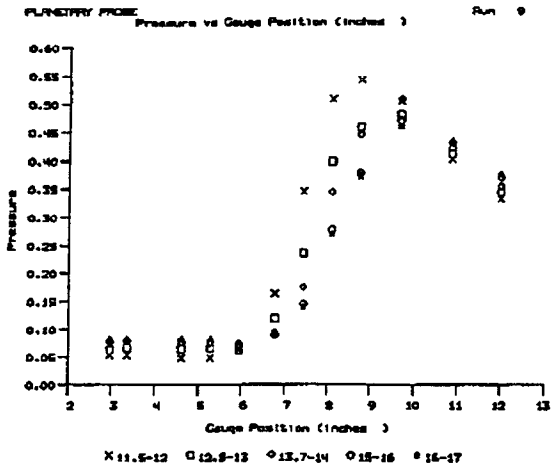

Figure 28 Time Establishment of Pressure Distribution Behind the Planetary Probe (Run 9)

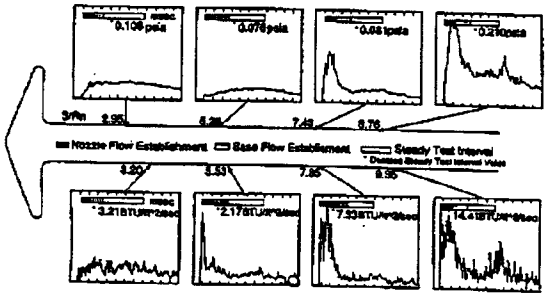

Figure 29 Time Histories of Pressure and Heat Transfer along Sting Behind Planetary Probe Showing Time Establishment

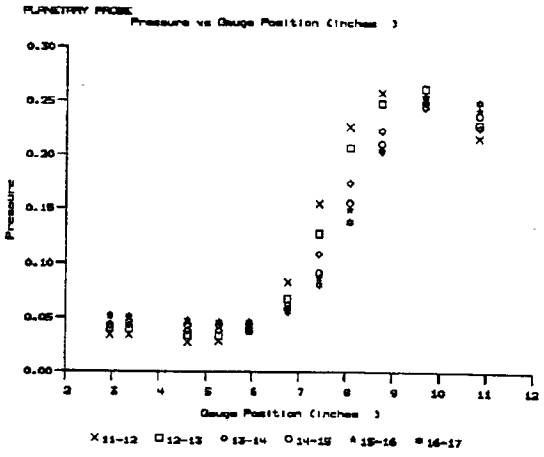

Figure 30 Time Establishment of Pressure Distribution Behind the Planetary Probe

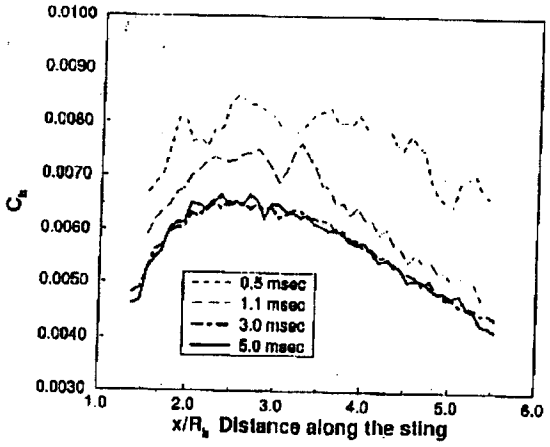

Figure 31 DSMC Prediction of Planetary Probe Flow Evolution of Heat transfer Along Sting

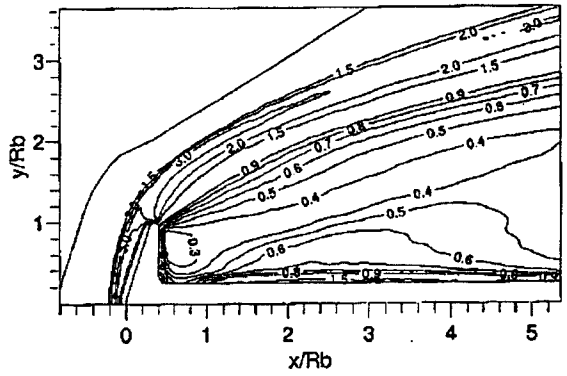

Figure 32a DSMC Predictions of Planetary Probe Flow Density Contour at 0.5 msec

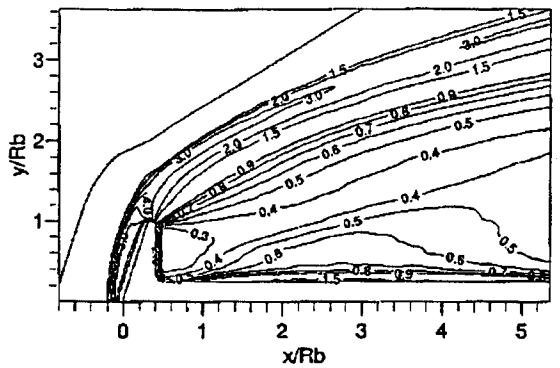

Figure 32b DSMC Predictions of Planetary Probe Flow Density Contours at 1.1 msec

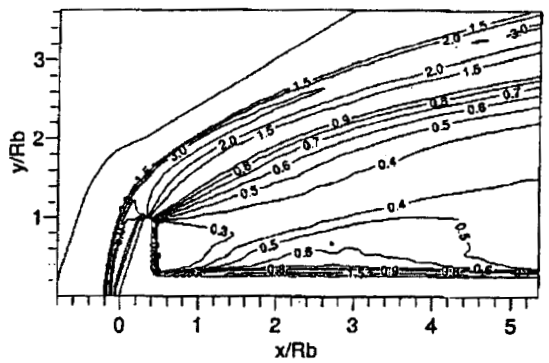

Figure 33a DSMC Predictions of Planetary Probe Flow Density Contours at 3.0 msecs

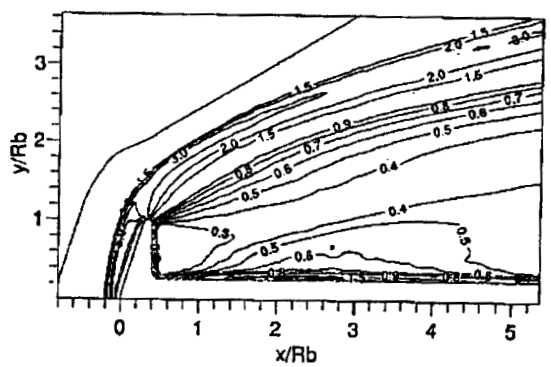

Figure 33b DSMC Prediction for Planetary Probe Flow Density Contour at 5.0 msec.

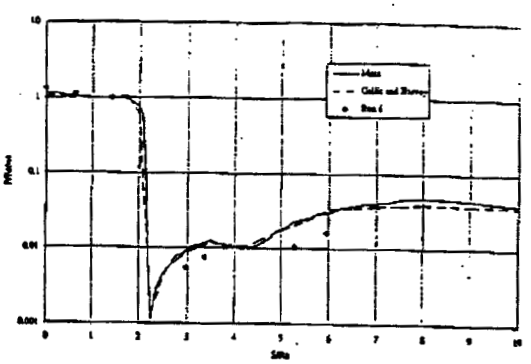

Figure 34a Comparison Between the Measured Pressure Distribution on Planetary Probe and DSMC Calculations by Moss (Ref. 7) and Gallis and Harvey (Ref. 6) for the LENS Case B Condition.

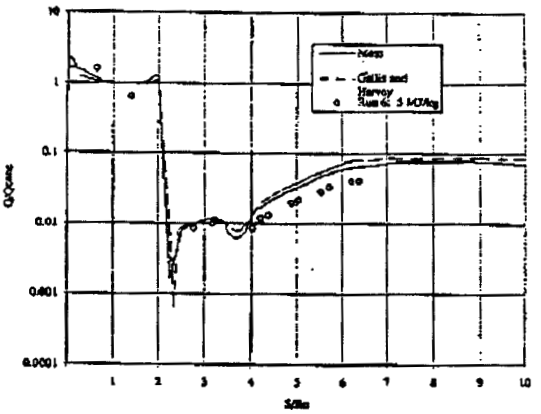

Figure 34b Comparison Between the Measured Heat Transfer Distribution on the Planetary Probe Configuration and Calculations by Moss (Ref. 7) and Gallis and Harvey (Ref. 6) for the LENS case B test condition.

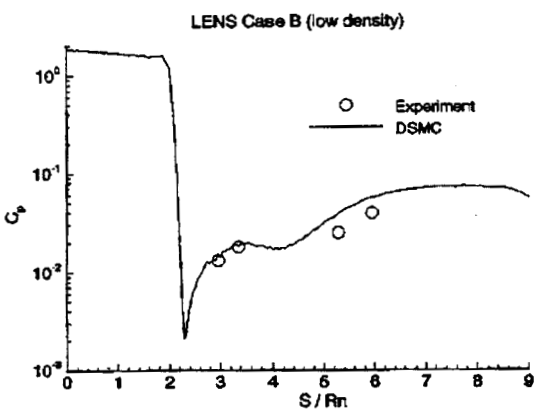

Figure 35a Comparison Between the Measured Pressure Distribution on Planetary Probe and DSMC Calculations by Dietrich and Boyd (Ref. 9) for the LENS Case B Condition.

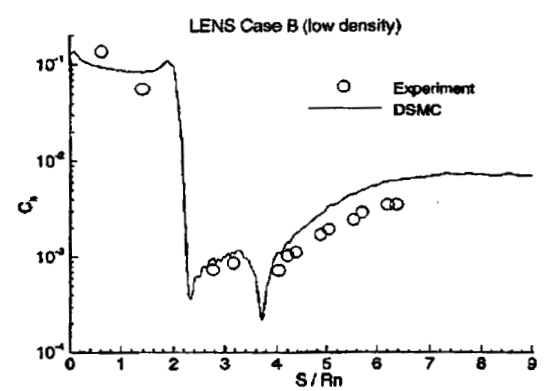

Figure 35b Comparison Between the Measured Heat Transfer Distribution on the Planetary Probe Configuration and Calculations by Dietrich and Boyd (Ref. 9) for the LENS Case B Test Condition

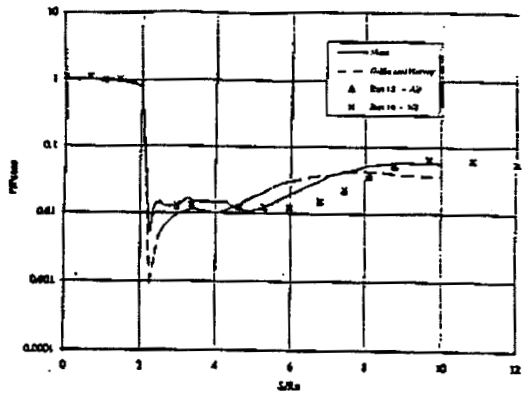

Figure 36 Comparisons Between the Measured Pressure Distribution and DSMC and Navier-Stokes Predictions by Gallis and Harvey(Ref 6) and Hassan (Ref. 10) for the LENS Case C Test Condition

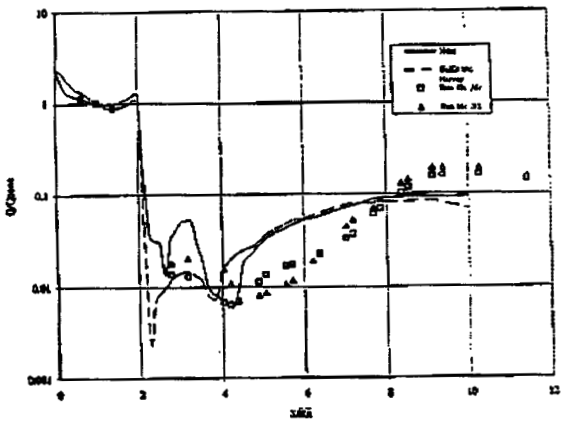

Figure 37 Comparisons between the Measured Heat Transfer Distribution and DSMC and Navier-Stokes Predictions by Gallis and Harvey(Ref. 6) and Hassan (Ref. 10) for the LENS Case C Test Condition

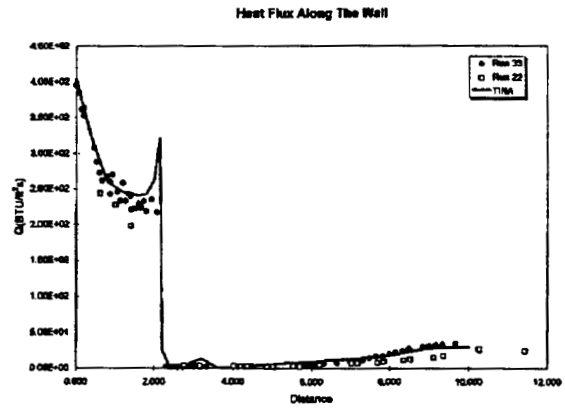

Figure 38 Comparison Between Calculations with "TINA" Navier-Stokes Code by Muylaert, et al. (Ref. 11) with Heat Transfer Measurements made in LENS Facility in Runs 22 and 33 at "Match Point" Case E

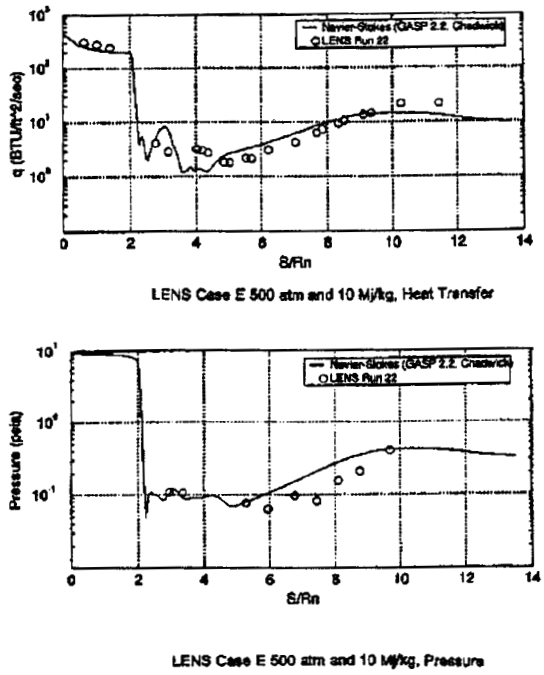

Figure 39 Comparison Between Calculations with the GASP Navier-Stokes Code by Chadwick, et al. (Ref. 12) with Heat Transfer and Pressure Measurements made in LENS Facility in Run 22 at "Match Point" Case E

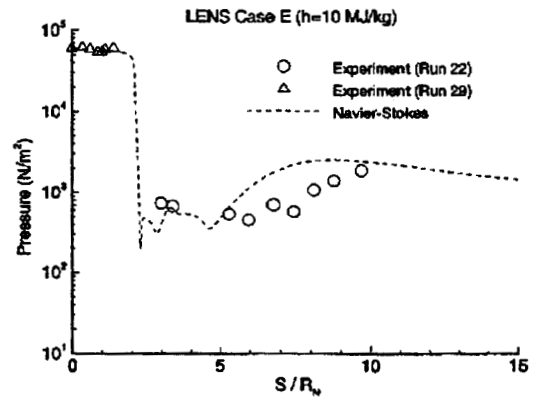

Figure 40 Comparison Between Calculations with the Cornell Navier-Stokes Code with Pressure Measurements made in LENS Facility in Runs 22 and 29 at "Match Point" Case E

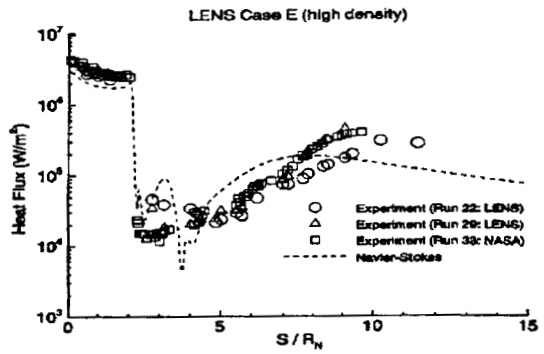

Figure 41 Comparison Between Calculations with the Cornell Navier-Stokes Code with Heat Transfer Measurements made in LENS Facility in Runs 22, 29 & 33 at "Match Point" Case E

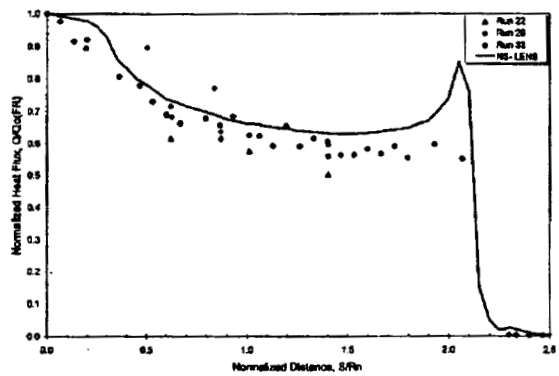

Figure 42 Comparison Between Calculations with Navier-Stokes Code by Gochberg with Normalized Heat Transfer Measurements made to the Front Face of the Planetary Probe in the LENS Facility in Runs 22, 29 & 33 at "Match Point" Case E

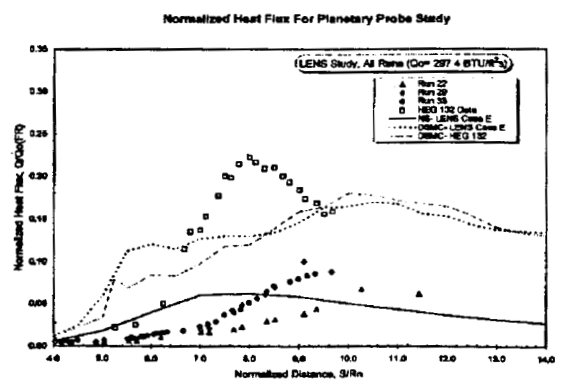

Figure 43 Comparison Between Calculations with Hybrid Navier-Stokes/DSMC Code by Gochberg with Normalized Heat Transfer Measurements made to the Rear Face and Sting of the Planetary Probe in the LENS Facility in Runs 22, 29 & 33 at "Match Point" Case E, including Measurements from HEG Run 132

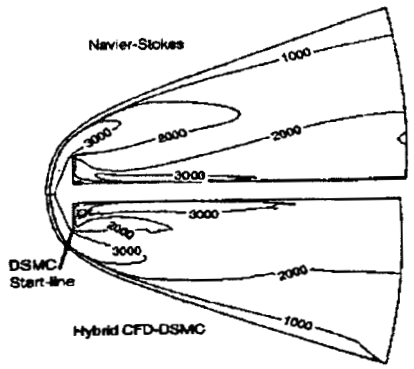

Figure 44 Flowfield Map Defining the Regions where Navier-Stokes and DSMC Calculations have been Overlapped for the Decoupled Navier-Stokes/DSMC Computations Performed at Cornell

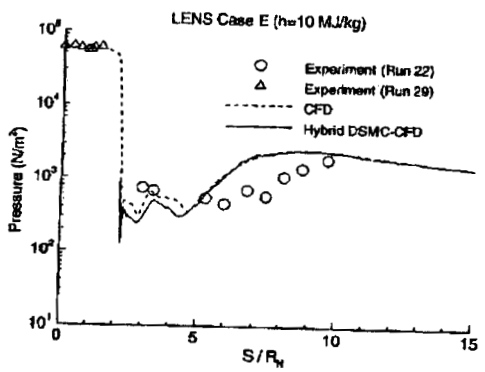

Figure 45 Comparison Between Pressure Measurements on Planetary Probe and Sting Configuration for LENS Case E and Calculations performed at Cornell Employing Decoupled Navier-Stokes/DSMC Calculations

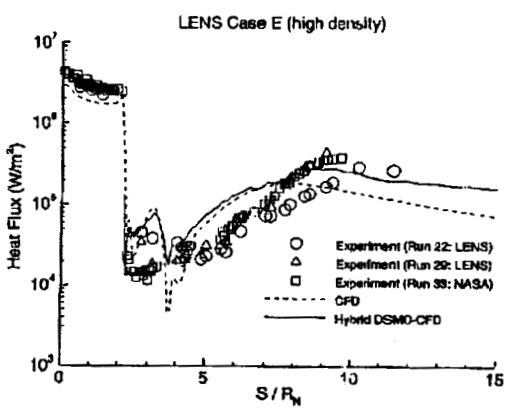

Figure 46 Comparison Between Heat Transfer Measurements on Planetary Probe and Sting Configuration for LENS Case E and Calculations Performed at Cornell Employing Decoupled Navier-Stokes/DSMC Calculations